ELSEVIER

European Journal of Radiology 65 (2008) 36–46

EJR
EUROPEAN JOURNAL OF RADIOLOGY

www.elsevier.com/locate/ejrad

Readout-segmented EPI for rapid high resolution diffusion imaging at 3T

Samantha J. Holdsworth [a], Stefan Skare [a], Rexford D. Newbould [a], Raphael Guzmann [b], Nikolas H. Blevins [c], Roland Bammer [a,*]

[a] *Lucas Center, Department of Radiology, Stanford University, 1201 Welch Road, Stanford, CA 94305-5488, USA*
[b] *Department of Neurosurgery, Stanford University, Stanford, CA, USA*
[c] *Department of Otolaryngology, Stanford University, Stanford, CA, USA*

Received 11 September 2007; accepted 12 September 2007

Abstract

Readout mosaic segmentation has been suggested as an alternative approach to EPI for high resolution diffusion-weighted imaging (DWI). In the readout-segmented EPI (RS-EPI) scheme, segments of *k*-space are acquired along the readout direction. This reduces geometric distortions due to the decrease in readout time. In this work, further distortion reduction is achieved by combining RS-EPI with parallel imaging (PI).

The performance of the PI-accelerated RS-EPI scheme is assessed in volunteers and patients at 3T with respect to both standard EPI and PI-accelerated EPI. Peripherally cardiac gated and non-gated RS-EPI images are acquired to assess whether motion due to brain pulsation significantly degrades the image quality. Due to the low off-resonance of PI-driven RS-EPI, we also investigate if the eddy currents induced by the diffusion gradients are low enough to use the Stejskal–Tanner diffusion preparation instead of the twice-refocused eddy-current compensated diffusion preparation to reduce TE.

It is shown that non-gated phase corrected DWI performs equally as well as gated acquisitions. PI-driven DW RS-EPI images with substantially less distortion compared with single-shot EPI are shown in patients—allowing the delineation of structures in the lower parts of the brain. A twice-refocused diffusion preparation was found necessary to avoid blurring in the DWI data. This paper shows that the RS-EPI scheme may be an important alternative sampling strategy to EPI to achieve high resolution T2-weighted and diffusion-weighted images.

Keywords: MRI; Echo-planar imaging; Diffusion-weighted imaging (DWI); Diffusion tensor imaging (DTI); Parallel imaging

1. Introduction

The distortions present in echo-planar imaging (EPI) images are governed mainly by the slow traversal through *k*-space along the phase-encoding direction [1]. The low bandwidth in this direction (note that the sampling rate along this dimension is essentially the echo spacing of the EPI train) gives rise to blurring and geometric distortions. These artifacts can be diminished significantly by accelerating the *k*-space traversal along the phase-encoding direction. One method is to use interleaved EPI, in which the distortions can be reduced by a factor that is equal to the number of interleaves used. An alternative to interleaving *k*-space along the phase-encoding direction is to partition *k*-space into segments along the readout direction. Initially referred to as mosaic segmentation [2], this approach was advanced by the use of multiple segments coupled with a navigator, and referred to as readout mosaic segmentation EPI (RS-EPI) [3]. In the RS-EPI scheme, *k*-space is covered with a break in the readout direction, filling *k*-space with several adjacent EPI segments or 'blinds' (see Fig. 1).

Both interleaved EPI and RS-EPI fill only a part of *k*-space after each diffusion preparation. Due to the unwanted phase error induced by motion during the diffusion gradients, each of these *k*-space segments are positioned slightly incorrectly in an arbitrary direction in *k*-space, which is why navigator echoes [4–6] are necessary to correct for this. However, following correction, interleaved EPI diffusion-weighted data may partially overlap in the phase-encoding direction, leading to gaps in *k*-space that cause ghosting artifacts in the image [5]. On the contrary, for RS-EPI, each blind is densely sampled in the phase-encoding direction at full Nyquist rate and is subject to the same phase error, thus navigator correction leaves only harmless gaps at the edges of *k*-space in the phase-encoding direction. Furthermore, with some overlap of

* Corresponding author. Tel.: +1 650 498 4760; fax: +1 650 723 5795.
E-mail address: rbammer@stanford.edu (R. Bammer).

0720-048X/$ – see front matter © 2007 Elsevier Ireland Ltd. All rights reserved.
doi:10.1016/j.ejrad.2007.09.016

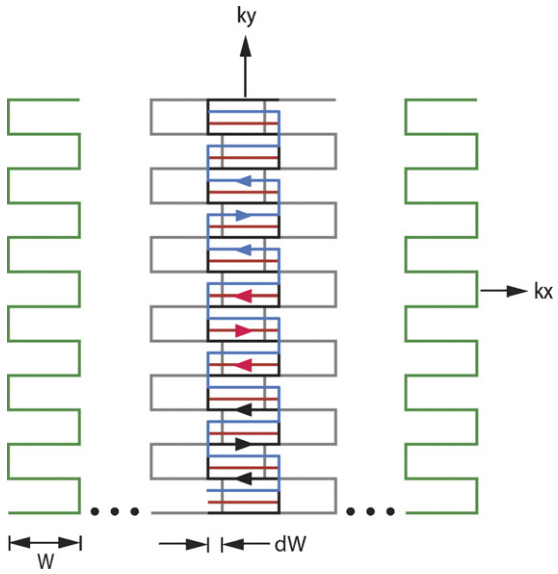

Fig. 1. *k*-Space trajectories for the RS-EPI sequence. *k*-Space is filled with an odd number of separate blinds, *B*, (indicated by green, grey, and black) of a given blind width, *W*, and overlapping factor, OF = d*W*/*W*. A fully sampled central blind (indicated by interleaved black, red, and blue trajectories) is used to get the ghost calibration parameters and GRAPPA weights, which are applied to all other blinds.

blinds, potential gaps in the readout direction can also be easily avoided.

One slight disadvantage of RS-EPI is a reduction of the 'effective' readout gradient strength [7]. On modern high-performance gradient systems, EPI data are acquired during the rising and falling edges of the readout gradient to shorten the overall readout time. With RS-EPI, the changes in readout gradient polarity occur more frequently than with regular single-shot (ss)EPI or interleaved EPI—thus only a fraction of the available maximum gradient strength gets utilized. Due to the lower 'effective' readout gradient, the *k*-space is read out slightly more slowly [7]. Therefore, in this paper RS-EPI is combined with parallel imaging to further speed up *k*-space traversal, compensating for the reduced gradient efficiency.

By combining RS-EPI with parallel imaging, diffusion-weighted images can be observed at 3T with spatial resolution comparable to conventional anatomical imaging at very low distortion levels. It is shown that any remaining observable distortions do not scale with the target resolution, making RS-EPI more competitive than EPI at higher resolutions. Peripherally cardiac gated and non-gated RS-EPI images are acquired to assess the image quality in the presence of pulsatile motion, and to demonstrate the effect of navigator correction. Standard ssEPI images, as well as EPI and RS-EPI images accelerated by parallel imaging (PI) are compared. In this work, the 2D GRAPPA PI method was used [8,9]. We demonstrate that a combination of the RS-EPI trajectory and parallel imaging results in high resolution T2-weighted and diffusion-weighted images with significantly reduced geometric distortions, acquired in a reasonable scan time. Clinical RS-EPI DWI and DTI images delineate tumors near the auditory canals, nasal cavity, and the brain stem—areas traditionally difficult for EPI-based trajectories to image with high quality.

2. Materials and methods

The RS-EPI spin echo-based diffusion pulse sequence timing diagram is shown in Fig. 2. Twice-refocused diffusion preparation was used to avoid potential eddy currents that can arise from the switching of the diffusion gradients [10]. For each repetition (TR), an imaging echo (or blind—as shown in Fig. 1) and its accompanying navigator echo are acquired. Each navigator echo is used only to sample the *central blind* of *k*-space. The imaging echo fills *k*-space with separate (adjacent or overlapping) blinds until the target resolution is reached. Depending upon the number of blinds chosen, *B*; the blind width, *W*; and the target resolution *N*—the amount the blinds may overlap, d*W*, is described by the overlapping factor, OF = 100% × d*W*/*W*.

For a given target resolution, the number of blinds should always be chosen so that the resulting overlapping factor is equal or greater than 0% (in other words: $B \geq N/W$) to avoid aliasing and ghosting in the readout-direction. For all datasets, however, an odd number of blinds were selected in order to provide a fully sampled central segment (with *R* interleaves) for FOV/2-ghost correction [11] and GRAPPA [8] calibration [12].

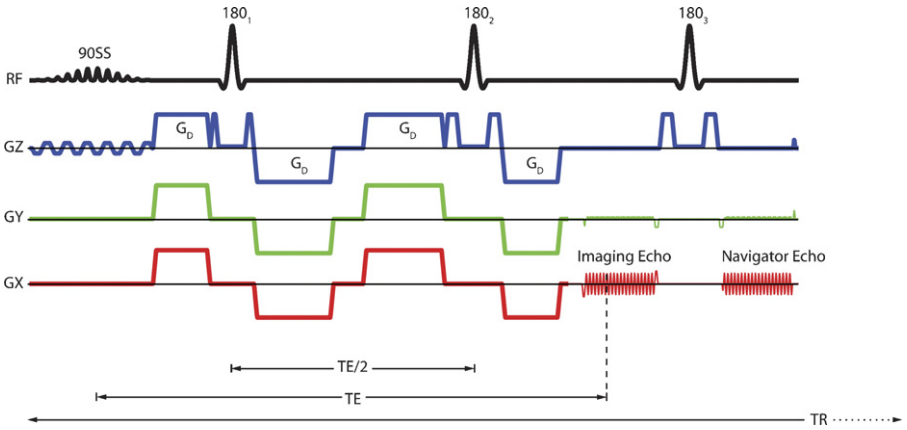

Fig. 2. Pulse sequence timing diagram for the RS-EPI, twice-refocused spin echo-based diffusion sequence. The RF pulses (spectral-spatial 90° and refocusing 180°); the diffusion gradients G_D; and the imaging and navigator echo are shown. TE is the echo time of the imaging echo, and TR is the sequence repetition time.

In order to reduce the echo time (TE), both echoes were acquired with partial Fourier encoding in the phase-encoding direction. The number of extra acquired *k*-space phase-encoding lines made up a total of $N_O = 18$ overscans (so that the number of extra lines made up $N_O/(N/2) \times 100\%$ of the maximum *k*-space radius).

The *k*-space data for all blinds were acquired during the rising and falling portions of the readout gradient and thereafter reconstructed [11]. Here, correction parameters for FOV/2 ghost correction and GRAPPA weights were determined from all *R* interleaves for the T2-weighted ($b = 0$ s/mm^2) middle blind, where *R* is the PI- or GRAPPA-acceleration factor. These calibration parameters and weights were applied to all other blinds. With the phase information obtained from the navigator echo (Fig. 2), the blinds were each phase corrected using a triangular windowing approach [13,14]. Complex averaging over the interleaves; gridding to combine all blinds in *k*-space [15]; and POCS reconstruction of the partial Fourier data [16,17] to fill in the remaining required extent of *k*-space – were performed for each coil. The final image was obtained via performing the sum of squares reconstruction over all coils.

All scans were performed on a 3T whole-body GE EXCITE system (Milwaukee, WI, USA) using an eight-channel head coil and a high-performance gradient system (40 mT/m, SLR = 150 mT/m/s). For human studies, datasets were acquired on both volunteers and patients. All procedures were approved by the institutional review board.

2.1. Volunteer measurements

Three healthy volunteers were scanned for the following experiments:

1. To assess the influence of peripheral cardiac gating *versus* no-gating, as well as phase correction *versus* no phase correction on image quality.
2. Distortion comparison between GRAPPA-accelerated EPI and RS-EPI, and ssEPI.
3. High resolution axial, sagittal, and coronal RS-EPI images.
4. Single *versus* twice refocused diffusion preparation to determine whether the echo time can be reduced.

In the following sections, the aforementioned experiments are described in more detail.

2.1.1. Peripheral cardiac gating versus no gating

If motion due to brain pulsations in multi-shot EPI-based techniques is large, the accumulation of phase errors due to the diffusion encoding gradients may result in severe dropouts in the final image—especially in the base of the brain around the fourth ventricle. In addition, RS-EPI requires the acquisition of several overlapping blinds and is thus more susceptible to phase errors caused by motion-induced phase mismatch between repeated excitation periods. These effects can be reduced significantly with the use of prospectively gated acquisitions: however – depending on heart rate – these can suffer from ∼10% up to ∼100% longer scan time [18]. Therefore, the first experiment was performed to assess whether RS-EPI diffusion acquisitions can be used without gating, providing a reliable and faster alternative to cardiac gated acquisitions.

RS-EPI images were acquired, both with and without peripheral cardiac gating, at a target resolution of $N = 288$, using $B = 7$ blinds of width $W = 64$ (OF = 36%). The acquisitions consisted of one $b = 0$ s/mm^2 and one $b = 1000$ s/mm^2, applied in the S/I (through-plane) direction only, (the most sensitive direction for signal loss [19]). Other imaging parameters were as follows: $R = 3$; number of averages (NEX) = 3; TE = minimum (68 ms); $N_O = 18$; TR = 3 RR intervals; readout duration per gradient echo = 268 μs; and FOV = 26 cm.

All RS-EPI datasets were reconstructed with and without the use of the navigator correction. When using navigator correction, each blind is corrected using the phase map [13] from its accompanying navigator echo.

2.1.2. Distortion comparison

The second experiment was performed to compare the level of distortion between conventional ssEPI data, and GRAPPA-accelerated RS-EPI and EPI. The GRAPPA-accelerated RS-EPI and EPI diffusion-weighted schemes were tested on a volunteer using $R = 3$ shots at two different target resolutions: 192×192 and 288×288. A blind width of 32 (OF ∼ 15%) was used for the RS-EPI data. Single-shot EPI data was acquired at the conventional resolution: 128×128, as well as at the same target resolutions as above. All schemes used positive phase-encoding blips; $N_O = 18$; the minimum echo time; a TR of 3 s; a slice thickness of 5 mm; NEX = *R*; and a FOV of 24 cm. The readout duration for one gradient echo was 196 μs, 456 μs, and 668 μs for a readout resolution of 32, 192, and 288, respectively. For RS-EPI the minimum TE was 68 ms, whilst the minimum TE for the 192×192 and 288×288 EPI with GRAPPA was 72 ms and 75 ms, respectively. For ssEPI without GRAPPA the TE was 95 ms and 113 ms. Since the distortion properties for the $b = 0$ and $b = 1000$ s/mm^2 are equivalent, only the $b = 0$ data was used for the distortion comparison. A fat-saturated FSE sequence was also implemented for geometric reference.

2.1.3. High resolution axial, sagittal, and coronal images

Axial, sagittal, and coronal RS-EPI $b = 0$ and $b = 1000$ s/mm^2 images were acquired on a volunteers at a target resolution of 288×288. Imaging parameters were: FOV = 24 cm; a slice thickness = 5 mm; TR/TE = 3 s/68 ms; $R = 3$; NEX = *R*; 9 blinds of width 64 (OF = 50%); isotropic tetrahedral encoding with $b = 1000$ s/mm^2. The scan time was 6:48 min for each of the three acquisitions.

2.1.4. Eddy currents: single versus twice refocused diffusion preparation

The increased speed of *k*-space traversal with the use of the short-axis RS-EPI trajectory implies that it may not be necessary to implement the twice refocusing intended for reducing eddy currents. Ruling out the requirement for twice refocusing can reduce the echo time by approximately 15 ms and enhance the SNR by ∼30%. Single and twice refocused GRAPPA-accelerated RS-EPI ($N = 288$, $R = 3$, $B = 7$, $W = 64$, OF = 36%)

datasets were acquired on a healthy volunteer using a 5 mm slice thickness. Both acquisitions consisted of one $b = 0$ s/mm^2 and seven $b = 1000$ s/mm^2 applied using a set of gradient vector directions isotropically distributed according to Coulomb's law of repulsion [20]. Isotropic DWI and fractional anisotropy maps are presented.

2.2. Patient measurements

The aim of the following experiments is to demonstrate the potential benefit of the use of high-resolution diffusion-weighted imaging in a clinical setting. RS-EPI acquisitions were performed in two patients with a brain stem cavernoma, and one with a cholesteatoma. All datasets were acquired without cardiac gating, using a FOV = 24 cm; TR = 3 s; partial-Fourier encoding with $N_O = 18$; and minimum echo time, as follows:

Patient #1 (cavernoma): RS-EPI ($N = 192$, $R = 3$, NEX = 3, $B = 5$, $W = 64$, OF = 40%) and ssEPI ($N = 128$) $b = 0$ s/mm^2 and three $b = 1000$ s/mm^2 DWI images in the x, y, and z direction were acquired using a slice thickness of 4 mm.

Patient #2 (cavernoma): An RS-EPI DTI dataset was acquired ($N = 192$, $R = 3$, $B = 7$, $W = 32$, OF = 14%) using a slice thickness of 5 mm. Diffusion weighting with a b-factor of 1000 s/mm^2 was carried out along 13 isotropically distributed directions, complemented by two $b = 0$ s/mm^2 images—leading to a total scan time of 16 min. Isotropic DWI (ISODWI), isotropic ADC (ISOADC), exponential ADC (EADC), fractional anisotropy (FA) maps, and directionally encoded color maps are presented. An FSE sequence acquired at an equivalent target resolution was also used for geometric reference.

Patient #3 (cholesteatoma): RS-EPI and Cartesian-EPI DWI datasets were acquired on a patient with a small cholesteatoma of the middle left ear, using an acceleration factor of $R = 3$ with diffusion gradients applied in the x, y, and z direction ($b = 1000$ s/mm^2). The two datasets were acquired at an equivalent target resolution of 288 × 288. The RS-EPI used 9 blinds ($W = 64$, OF = 50%), while the EPI sequence used 9 repetitions of the diffusion scheme to make the scan time equivalent (5.4 min each). A fluid-attenuated inversion recovery (FLAIR), FSE, and

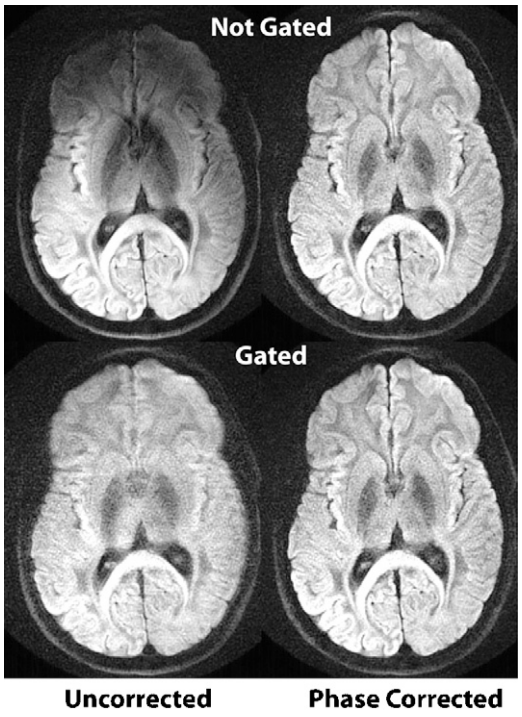

Fig. 3. RS-EPI DWI gated and non-gated datasets ($b = 1000$ s/mm^2, S/I direction) acquired with a target resolution of $N = 288$, using $R = 3$ interleaves; NEX = 3 averages; $B = 7$ blinds of width $W = 64$—giving a blind overlapping factor OF = 36%. Both datasets are reconstructed both with and without phase correction. Other imaging parameters were: FOV = 24 cm; slice thickness = 5 mm; TR = 3 s and a scan time of 65 s.

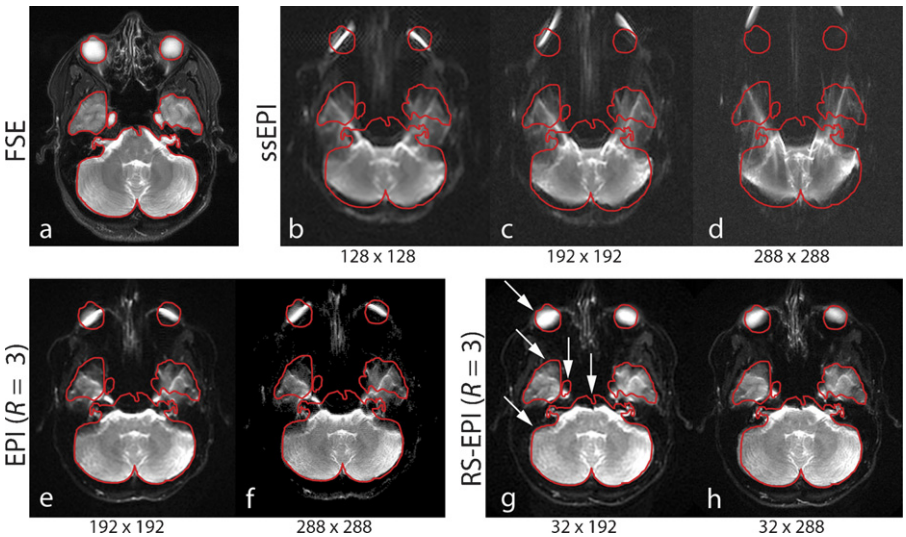

Fig. 4. T2-weighted ($b = 0$ s/mm^2) images of a healthy volunteer, showing (a) a negligibly distorted FSE image onto which contour lines are drawn. These contour lines are transferred to (b–d) ssEPI images; (e, f) $R = 3$ EPI; and (g, h) $R = 3$ RS-EPI datasets. The EPI and RS-EPI acquisitions are acquired with different target resolutions as shown ($N = 192$ and 288), using a FOV = 24 cm, a slice thickness = 5 mm, NEX = 3, a TR = 3 s, and the minimum TE with partial Fourier encoding with $N_O = 18$. The RS-EPI datasets were acquired with a blind width $B = 32$, using (g) $B = 7$ (OF = 14%), and (h) $B = 11$ (OF = 18%). The white arrows on the RS-EPI image in (g) show regions of improved distortion properties compared with EPI.

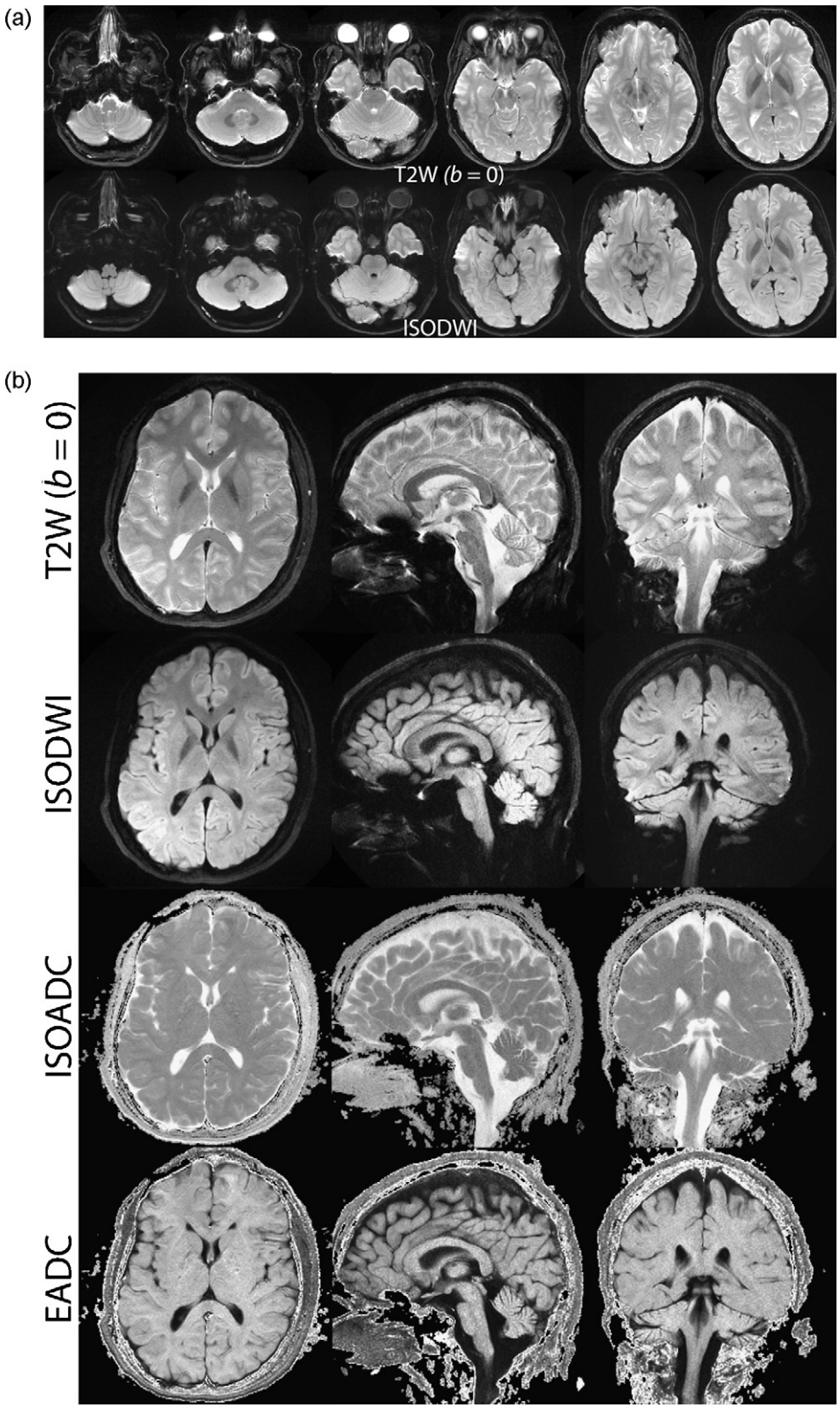

Fig. 5. RS-EPI $b = 0$ and $b = 1000\ s/mm^2$ (isotropic tetrahedral encoding) images, where (a) shows six axial slices of one volunteer and (b) shows three planes (axial, sagittal, and coronal) acquired from a second volunteer. Imaging parameters for both datasets are: FOV = 24 cm, slice thickness = 5 mm, $N = 288$, $R = 3$, NEX = 3, $B = 9$, $W = 64$, OF = 50%, TR/TE = 3 s/62 ms, scan time = 6:48 min for each acquisition.

spoiled-gradient-echo images were also acquired for geometric reference.

3. Results

Fig. 3 shows RS-EPI diffusion-weighted images acquired with and without gating, as well as with and without phase correction. As shown in the left column of Fig. 3, image degradation due to brain motion (e.g. pulsation) during the application of the diffusion-encoding gradients is evident in both acquisitions when phase correction is turned off, although the gated acquisition shows a less pronounced signal dropout. However, applying the triangular-window phase correction with the use of the navigator echo restores image quality, regardless of the use of gating.

The distortion comparison between ssEPI, and GRAPPA-accelerated EPI and RS-EPI $b = 0$ datasets is shown in Fig. 4. The FSE image (Fig. 4a) was used as a reference for the distortion comparison. On this image, a contour was drawn in red around the brain structures. These contours were transferred to all other images to allow a pixelwise comparison of the geometry for ssEPI (Fig. 4b–d); $R = 3$ GRAPPA-accelerated EPI (Fig. 4e and f); and $R = 3$ RS-EPI (Fig. 4g and h). Due to the long EPI readout train and echo spacing, the ssEPI datasets are prone to considerable levels of distortion and blurring. As can be seen, there is little advantage in increasing the target resolution of ssEPI beyond 128×128, since the resulting images are dominated by geometric distortions. These distortions are dramatically reduced with the use of the GRAPPA acceleration (Fig. 4e and f). Further reduction in blurring and distortion is evident in the RS-EPI images (Fig. 4g and h), especially at the level of the brain stem and the eyes. Scan times of all applied EPI sequences are summarized in Table 1. The increased readout length could potentially introduce blurring for RS-EPI due to T2* decay as the resolution is increased. However, comparing 192 and 288 (Fig. 4g and h), this effect seems to be undetectable. Further demonstration of the high resolution images achievable with the RS-EPI sequence is shown in Fig. 5a and b. Here, RS-EPI $b = 0\ s/mm^2$ and isotropically weighted $b = 1000\ s/mm^2$ images acquired at an in-plane target resolution of $0.8\ mm^2$ (matrix size 288×288) present with little blurring and distortion in all three planes.

Fig. 6 shows the results from comparing conventional Stejskal–Tanner (single-refocused) diffusion-weighted spin-echo imaging with a twice-refocused approach. In both cases, the GRAPPA-accelerated RS-EPI method was used. Despite the significantly increased bandwidth per pixel along the phase-encoding direction, the diffusion-weighted spin-echo RS-EPI with conventional spin-echo refocusing demonstrates noticeable spatial misregistration effects—which resulted in image blurring; whilst the twice-refocused approach was essentially free from distortions induced by eddy-current based field perturbations.

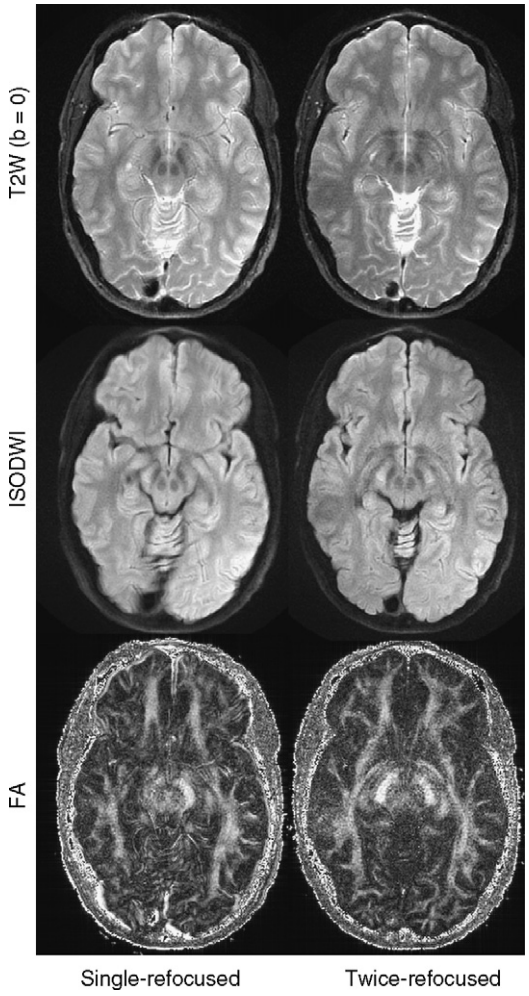

Fig. 6. Single- and twice-refocused RS-EPI DTI datasets (one $b = 0\ s/mm^2$ direction, and seven $b = 1000\ s/mm^2$ directions). Imaging parameters for both datasets were: $N = 288$, $R = 3$, NEX = 3, $B = 7$, $W = 64$, OF = 36%, partial Fourier encoding with $N_O = 18$, FOV = 24 cm, slice thickness = 5 mm, and a TR = 3 s. The TE was (left) 60 ms and (right) 67 ms.

Clinically relevant datasets of a patient presenting with a brain stem cavernoma are shown in Fig. 7. Corresponding anatomi-

Table 1
Scan time for isotropic diffusion-weighted ssEPI (NEX = 1), and GRAPPA-accelerated EPI and RS-EPI ($R = 3$, NEX = 3) acquisitions

Target resolution (N)	Scan time (min)			
	ssEPI	EPI ($R = 3$)	RS-EPI ($R = 3$, $W = 64$)	RS-EPI ($R = 3$, $W = 32$)
128	0:37*	0:60	1:80 ($B = 3$)	3:00 ($B = 5$)
192	0:67*	0:82*	1:92 ($B = 3$)*	4:20 ($B = 7$)*
288	1:27*	1:40*	4:30 ($B = 5$)*	5:94 ($B = 9$)*

Two blind widths (W) and the corresponding number of blinds (B) required to achieve the minimum overlap are shown for RS-EPI. Scan times are normalized for whole brain coverage (21 slices) using a TR = 3 s. Entries marked with an * represent acquisitions used in this work.

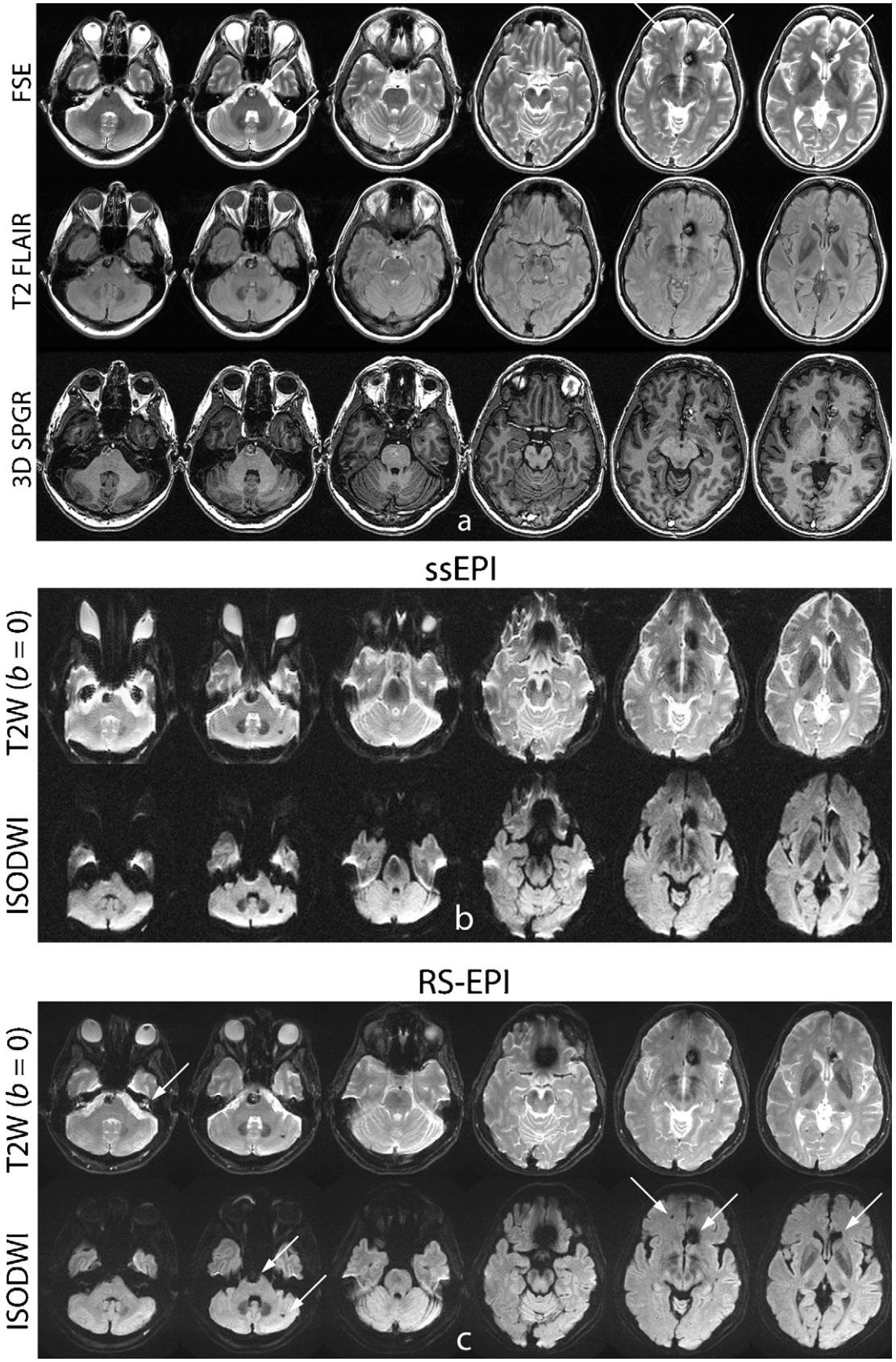

Fig. 7. (a) FSE, T2 FLAIR, and 3D spoiled-gradient-echo (SPGR) images acquired on a brain stem cavernoma patient. (b) ssEPI ($N = 128$) and (c) RS-EPI ($N = 192$) $b = 0$ s/mm^2 and isotropic DWI datasets (x, y, z direction, $b = 1000$ s/mm^2). (b and c) are acquired with a FOV = 24 cm, a slice thickness = 4 mm, and a TR = 3 s. The RS-EPI dataset is acquired with $R = 3$, NEX = 3, $B = 5$, $W = 64$, OF = 40%. The white arrow displayed on the $b = 0$ RS-EPI dataset depicts the 8th cranial (acoustic) nerve. The arrows on the FSE and ISODWI images also display additional lesions.

cal scans are shown in Fig. 7a, whilst ssEPI and RS-EPI DWI scans are shown in Fig. 7b and c. While the standard 128 × 128 ssEPI $b = 0\ s/mm^2$ and isotropically weighted $b = 1000\ s/mm^2$ images suffer from substantial distortion and blurring, the RS-EPI images clearly delineate both the brain stem cavernoma and other smaller lesions evident throughout the brain. Although the base of the brain is already a region of poor B0 homogeneity, the improvement in the RS-EPI is particularly noticeable in regions of even higher magnetic susceptibility variation—such as the regions around the nasal cavity, auditory canals and areas adjacent to the hemorrhagic lesions. In these areas, it can be difficult to resolve regions of distortion from the actual lesion.

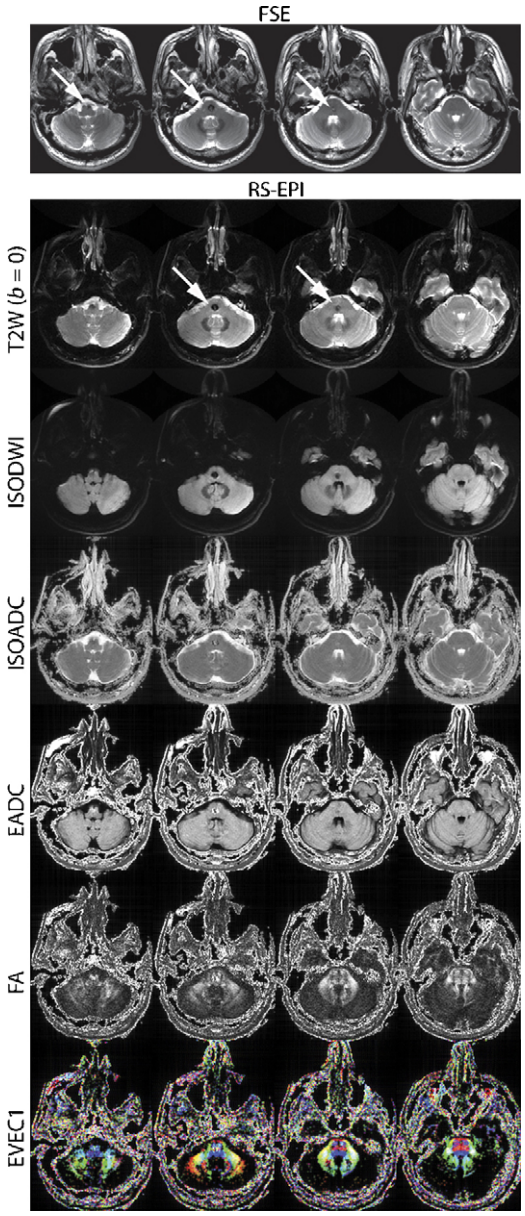

Fig. 8. A brain stem cavernoma patient showing an FSE ($N = 288$) (top); RS-EPI DTI dataset (bottom). The RS-EPI dataset set is acquired with two $b = 0$ images and 13 $b = 1000\ s/mm^2$ directions with $N = 192$, $R = 3$, NEX = 3, $B = 7$, $W = 32$, OF = 14%, TR/TE = 3 s/75 ms, $N_O = 18$, in a scan time of 16 min. Both datasets used a FOV = 24 cm and a slice thickness = 5 mm.

Another example for the outstanding image quality of the RS-EPI method is the delineation of the 8th cranial (acoustic) nerve on the $b = 0\ s/mm^2$ RS-EPI scan in Fig. 7c (arrowhead), while the ssEPI image in Fig. 7b displays complete dropout of this region altogether.

Another comparison is presented in Fig. 8, showing datasets of the second patient suffering from a brain stem cavernoma. RS-EPI DTI datasets of this patient show high SNR, high resolution images with little distortion—in an area which, again, is traditionally difficult for EPI-based trajectories to image with reliable image quality. A minimum level of geometric distortions and dramatically reduced sensitivity to blood products are paramount for this region—in order to provide the neurosurgeon with reliable information about fiber tract orientation/displacement to facilitate treatment planning.

A further comparison between GRAPPA-accelerated RS-EPI and EPI images ($R = 3$) of a cholesteatoma patient acquired in the same scan time is shown in Fig. 9. It has been reported that DWI is a sensitive method to pick up such lesions—most likely because of increased cellularity and thus decreased diffusivity [21]. While the lesion is not easily seen on the EPI image (Fig. 9b), the white arrows displayed on the RS-EPI dataset (Fig. 9c) depict a moderately hyperintense lesion on the $b = 0$ and $b = 1000\ s/mm^2$ images, suggesting the presence of a small cholesteatoma.

4. Discussion

Geometric distortions are unequivocally regarded as the main problem associated with single-shot EPI readout trajectories. However, other undesired effects such as T2* blurring and distortions emanating from eddy-current-induced field perturbations (especially for diffusion tensor imaging) need to be considered similarly. The magnitude of these artifacts in EPI is inversely scaled by the speed with which k-space is traversed along the phase-encoding direction, as k-space velocity (dk/dt) determines the bandwidth per pixel. These distortions linearly increase with field strength and, if not accounted for, severely reduce the benefits from migrating towards higher polarization fields.

The performance of EPI-based methods can be improved greatly when the distortions are mitigated by the use of sampling strategies such as interleaved EPI or RS-EPI, particularly when combined with parallel imaging. With RS-EPI, the short readout length of the individual blinds results in a considerable increase in k-space velocity along the phase-encoding direction compared to regular EPI, while it is immune to the motion-related ghosting issues of interleaved EPI. The degree of distortion is reduced by a ratio which is essentially proportional to the ratio of the full readout length to the blind width W. Also, since the maximum number of phase-encoding steps does not have any impact on the bandwidth per pixel along the phase-encoding direction, increasing the resolution in RS-EPI can be decoupled from additional artifacts, except for some additional T2* decay due to longer total readout time.

Despite the significantly increased bandwidth per pixel along the phase-encoding direction, eddy currents present in the Stejskal–Tanner (single-refocused) diffusion preparation were

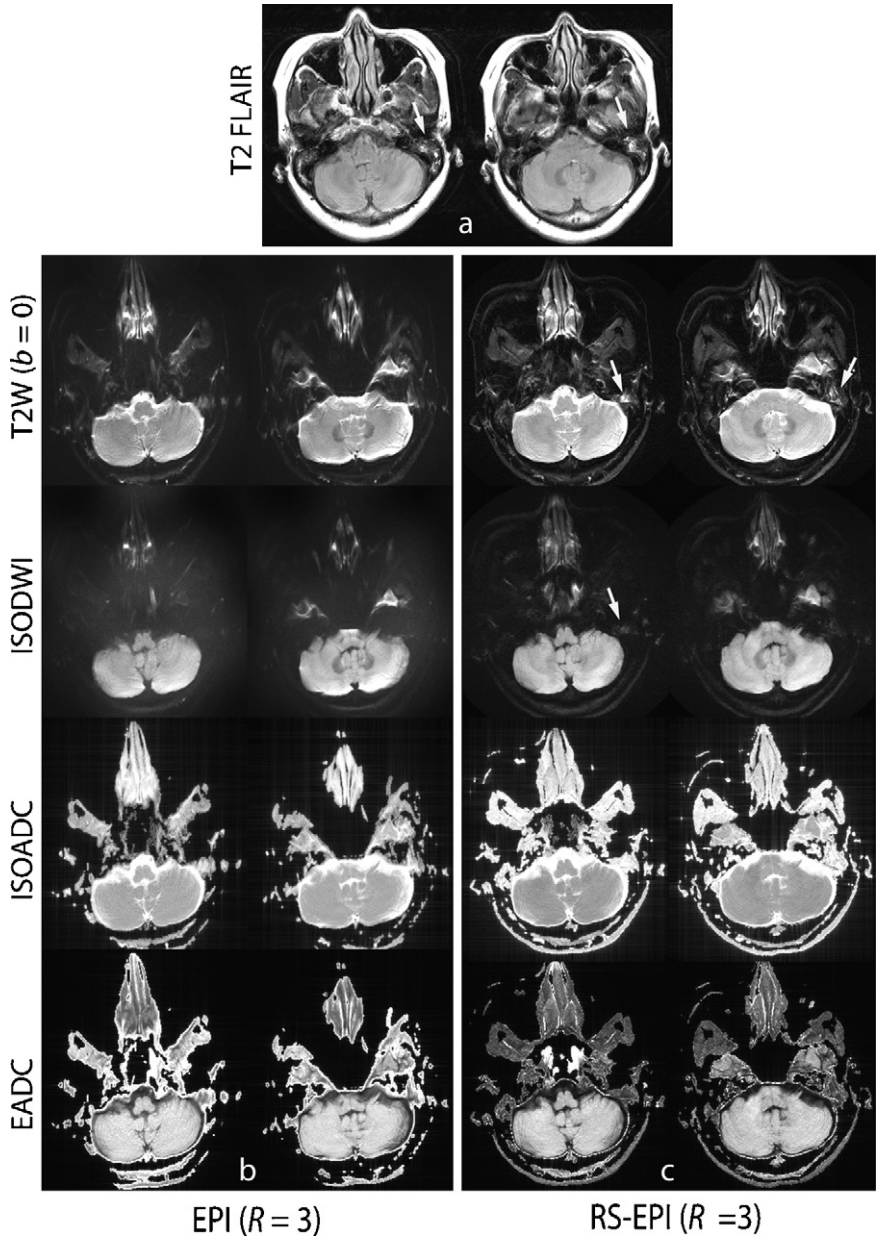

Fig. 9. (a) T2 FLAIR ($N = 288$) acquired on a cholesteatoma patient. The white arrows indicate a small lesion in the middle left ear. (b) EPI ($N = 288$, $R = 3$, NEX = 3) and (c) RS-EPI $b = 0$ and isotropic $b = 1000\,\text{s/mm}^2$ datasets (x, y, z direction), both acquired with $N = 288$, $R = 3$, and NEX = 3. The RS-EPI dataset is acquired with $B = 9$, $W = 64$, and OF = 50%. The EPI dataset is acquired with 9 repetitions resulting in a scan time of 5:24 min for both datasets. All datasets were acquired with a FOV = 25 cm and a slice thickness of 5 mm. The white arrows displayed on the RS-EPI dataset depict a moderately hyperintense lesion on the $b = 0$ and $b = 1000\,\text{s/mm}^2$ image, suggesting the presence of a small cholesteatoma.

visible in the form of blurring in the DWI data. Eddy current correction schemes may alleviate the requirement for single-refocusing—allowing shorter TEs and thus images with a higher signal-to-noise ratio and more slices per TR.

Brain motion present during the application of the diffusion-encoding gradients introduces phase shifts across the tissue, which conflicts with regular gradient encoding. Further complications may arise with partial *k*-space techniques, as the DC component of the *k*-space signal may be displaced outside the *k*-space sampling range—causing dramatic signal loss and large dropouts, especially in the base of the brain where the motion is highest [22]. However, in the experiments performed, this likelihood was reduced significantly by using 16 or more overscans (data not shown). Prospectively peripherally cardiac-gated sequences can be used to reduce the effect of these signal losses, whereby the imaging echo is acquired only in the time between two heartbeats when brain motion is smallest. However, we show that cardiac gated RS-EPI acquisitions may still be hampered by considerable artifacts due to brain motion. Furthermore, although slightly more SNR is lost in *non-gated* acquisitions, the resulting phase-corrected images are comparable to those of phase-corrected *gated* acqui-

sitions. Other simulations with both gated and non-gated data (not shown) show that, as long as the overlapping factor of consecutive blinds is equal to or greater than 0%, the final phase-corrected images have been essentially free from motion artifacts. In summary, phase-corrected non-gated RS-EPI acquisitions result in a significant scan time reduction compared to gated acquisitions—while rendering images with comparable quality. In both cases, however, it still may be wise to use an overlapping factor >0% to avoid gaps in *k*-space that may arise from motion-induced phase shifts of the individual blinds for diffusion-weighted acquisitions. Overlapping blinds help to avoid these gaps, enabling the correction of phase shifts in image space.

Recently, FSE approaches have been introduced, such as PROPELLER DWI, demonstrating superb image quality—as FSE is robust against susceptibility distortions and eddy-current effects due to RF refocusing [13]. However, the requirement for large-flip-angle FSE trains to control for effects from unwanted non-CPMG signal components [14,23,24] can raise problems at higher magnetic field strengths where the specific absorption rate (SAR) issues and B1 inhomogeneities increase. These factors, in conjunction with a significantly longer readout, can limit the number of slices and the overall performance of the sequence [25]. In these situations, the reduced distortions and minimum SAR of RS-EPI might pose an attractive alternative to FSE-based DWI. With the reduction of the echo time, readout length, and echo spacing in RS-EPI, high-resolution images can be acquired with very little distortion even around hemorrhage (Figs. 7 and 8) or metal. On the other hand, RS-EPI requires the acquisition of several adjacent EPI segments and an extra navigator, resulting in a longer scan time compared with ssEPI. For example, whole brain coverage (21 slices, TR = 3 s) acquired with isotropic diffusion-weighted ssEPI takes 67 s and 1:27 min for a target resolution of 192 × 192 and 288 × 288, respectively. For the same target resolutions, a GRAPPA-accelerated EPI acquisition ($R = 3$, NEX = 3) takes 82 s and 1:40 min, while a RS-EPI acquisition takes 4:20 min and 5:94 min ($R = 3$, NEX = 3, $W = 32$, OF = 10%). This is the new dilemma we are facing that, for high resolution diffusion tensor imaging, one must be willing to spend more time.

5. Conclusions

While the use of parallel imaging in combination with EPI has shown to improve geometric distortions in high resolution diffusion MRI, further reduction is made possible through the use of alternative sampling strategies such as RS-EPI. This pseudo-Cartesian sampling scheme has an advantage over radially-based *k*-space sampling strategies in that fewer blinds are required, resulting in a shorter scan time.

It was demonstrated that the combination of parallel imaging and the RS-EPI *k*-space trajectory gives improved diffusion-weighted images at 3T—resulting in images with reduced geometric distortions and exquisite spatial resolution. Clinical data show lesions in the lower part of the brain otherwise not detectable in standard ssEPI and PI-accelerated EPI.

Acknowledgements

The authors acknowledge grant support from the NIH (R01EB002711, R01NS047607, R01NS34866, P41RR09784), Swedish Research Council (K2007-53P-20322-01-4), the Lucas foundation, and the Oak foundation. The authors are grateful to Anne Sawyer and Sandra Rodriguez for providing assistance with the patient studies.

References

[1] Farzaneh F, Riederer SJ, Pelc NJ. Analysis of T2 limitations and off-resonance effects on spatial resolution and artifacts in echo-planar imaging. Magn Reson Med 1990;14:123–39.
[2] Robson MD, Anderson AW, Gore JC. Diffusion-weighted multiple shot echo planar imaging of humans without navigation. Magn Reson Med 1997;38:82–8.
[3] Porter D, Mueller E. Multi-shot diffusion-weighted EPI with readout mosaic segmentation and 2D navigator correction. In: 11th Proc Intl Soc Mag Reson Med. 2004. p. 442.
[4] Atkinson D, Porter DA, Hill DLG, Calamante F, Connelly A. Sampling and reconstruction effects due to motion in diffusion-weighted interleaved echo planar imaging. Magn Reson Med 2000;44(1):101–9.
[5] Butts K, de Crespigny A, Pauly JM, Moseley M. Diffusion-weighted interleaved echo-planar imaging with a pair of orthogonal navigator echoes. Magn Reson Med 1996;35:763–70.
[6] Liu C, Bammer R, Kim D, Moseley ME. Self-navigated interleaved spiral (SNAILS): application to high-resolution diffusion tensor imaging. Magn Reson Med 2004;52:1388–96.
[7] Skare S, Newbould RD, Clayton DB, Bammer R. Propeller EPI in the other direction. Magn Reson Med 2006;55:1298–307.
[8] Griswold MA, Jakob PM, Heidemann RM, et al. Generalized autocalibrating partially parallel acquisitions (GRAPPA). Magn Reson Med 2002;47:1202–10.
[9] Qu P, Shen GX, Wang C, Wu B, Yuan J. Tailored utilization of acquired *k*-space points for GRAPPA reconstruction. J Magn Reson 2005;174(1):60–7.
[10] Reese TG, Heid O, Weisskoff RM, Wedeen VJ. Reduction of eddy-current-induced distortion in diffusion MRI using a twice-refocused spin echo. Magn Reson Med 2003;(49):177–82.
[11] Nordell A, Bammer R, Skare S. Major speed-up of Nyquist ghost correction in ramp-sampled EPI. In: 15th Proc Intl Soc Mag Reson Med. 2007. p. 1833.
[12] Skare S, Newbould RD, Clayton DB, Albers GW, Nagle S, Bammer R. Clinical multishot DW-EPI through parallel imaging with considerations of susceptibility, motion, and noise. Magn Reson Med 2007;57(5):881–90.
[13] Pipe JG. Motion correction with PROPELLER MRI: application to head motion and free-breathing cardiac imaging. Magn Reson Med 1999;42:963–9.
[14] Pipe JG, Farthing VG, Forbes KP. Multishot diffusion-weighted FSE using PROPELLER MRI. Magn Reson Med 2002;47(1):42–52.
[15] Jackson JI. Selection of a convolution function for Fourier inversion using gridding. IEEE Trans Med Imag 1991;10:473–8.
[16] Haacke EM, Lindskog ED, Lin W. A fast, iterative, partial-Fourier technique capable of local phase recovery. J Magn Reson 1991;92:126–45.
[17] Liang ZP, Boada FE, Constable RT, Haacke EM, Lauterbur PC, Smith MR. Constrained reconstruction methods in MR imaging. Rev Magn Reson Med 1992;4:67–185.
[18] Skare S, Andersson JL. On the effects of gating in diffusion imaging of the brain using single shot EPI. Magn Reson Imag 2001;19(8):1125–8.
[19] Wirestam R, Greitz D, Thomsen C, Brockstedt S, Olsson MB, Stahlberg F. Theoretical and experimental evaluation of phase-dispersion effects caused by brain motion in diffusion and perfusion MR imaging. J Magn Reson Imag 1996;6(2):348–55.
[20] Jones DK, Horsfield MA, Simmons A. Optimal strategies for measuring diffusion in anisotropic systems by magnetic resonance imaging. Magn Reson Med 1999;42(3):515–25.

[21] Reddy JS, Mishra AM, Behari S, et al. The role of diffusion-weighted imaging in the differential diagnosis of intracranial cystic mass lesions: a report of 147 lesions. Surg Neurol 2006;66(3):246–50 [discussion 50-1].
[22] Wedeen VJ, Weisskoff RM, Poncelet BP. MRI signal void due to in-plane motion is all-or-none. Magn Reson Med 1994;32(1):116–20.
[23] Alsop DC. Phase insensitive preparation of single-shot RARE: application to diffusion imaging in humans. Magn Reson Med 1997;38(4):527–33.
[24] Bammer R, Augustin M, Simbrunner J, Stollberger R, Fazekas F. Diffusion-weighted imaging of the spinal cord: interleaved EPI is superior to FSE. J Magn Reson Imag 2002;15:364–73.
[25] Holdsworth SJ, Bammer R, Newbould RD, Skare S. Benchmarking SAP-EPI and PROPELLER for diffusion imaging. In: 15th Proc Intl Soc Mag Reson Med. 2007. p. 1494.